

ON THE INFLUENCE OF TURBULENCE ON THE INITIATION OF SEDIMENT MOTION

U.C.E. ZANKE¹

ABSTRACT

For the initiation of sediment motion a theory is developed, which presupposes that the critical shear stress τ_c responsible for inducing motion in non-turbulent flow is solely defined by the angle of internal friction ϕ or the angle of repose ϕ' of single grains. In turbulent flow, fluctuations τ' in the shear stress as well as lift forces produced by these fluctuations also occur. Owing to this, the actual (effective) critical shear stress $\tau + \tau'$ acting on a grain is larger than the average stress τ on the one hand, and on the other hand, the effective weight of the grains is reduced: they become effectively lighter. On the basis of the presented analytical formulation the initiation of sediment motion may be described solely by the angle of repose of the grains and turbulence parameters.

Key Words: Critical shear stress, Angle of repose, Initiation of sediment motion, Turbulence parameter

1 PROBLEM DEFINITION

Owing to the practical importance of the initiation of motion many researchers began to tackle this problem even at the beginning of the last century (e.g. Kramer (1932, 1935), Casey (1935)). Shields (1936, Fig. 1) developed a non-dimensional representation based on the measured data of Casey, Kramer, USWES and Gilbert, together with his own data based on investigations with succinite sand, lignite, granite chips and heavy spar. Despite the different material properties, all of these results were found to lie within a single curve band. The non-dimensional parameters of the Shields diagram are the *critical non-dimensional shear stress* τ^* and the *Reynold's number of the grain* Re_d^* . The definition of τ^* is formulated as the ratio of the shear force F_T parallel to the bed to the weight F_W of the volume of material subjected to this shear force in the upper bed layer:

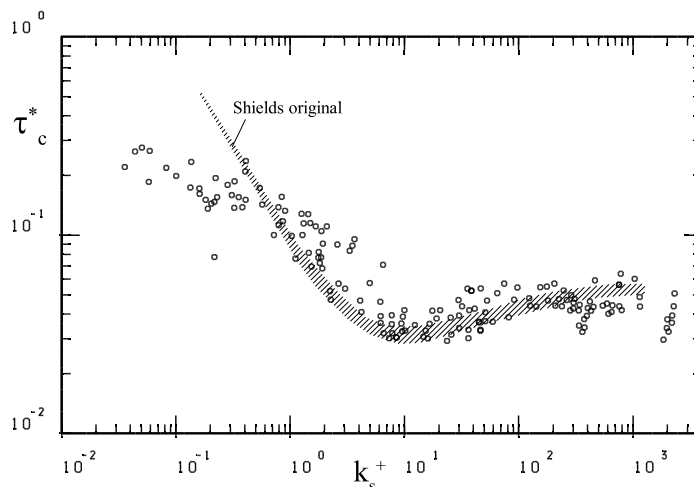


Fig. 1 Initiation of motion after Shields (1936) with additional data of Kramer, Uswes, Casey, Mantz (1977), Yalin/Karahan, Pазis and Unsöld

¹ Prof., Institute of Hydraulic Engineering, University of Technology, Darmstadt, Germany, E-mail: Zanke@aol.com
Notes: The manuscript of this paper was received in Nov. 2001. The revised version was received in Oct. 2002.
Discussion open until March 2004.

$$\tau^* = \frac{\tau}{(\rho_s - \rho)gd} = \frac{u^{*2}}{\rho'gd} = \text{const} \frac{F_T/A}{F_W/A} \quad (1)$$

In this formulation τ = the shear stress acting on the bed, ρ = density of the fluid, ρ_s = density of the sediment, $\rho' =$ relative density = $(\rho_s - \rho)/\rho$, d = grain diameter, g = gravitational acceleration and u^* = shear velocity. In Eq. 1, F_W represents the weight of a layer of the bed surface with a thickness of one grain diameter. The value of 'const.' depends on the solid material fraction. The value of approx. 0.7 for natural sediments (approx. 30% porosity) is adopted here as a reference value. The grain Reynold's number Re_d^* is given by

$$Re_d^* = \frac{u^*d}{\nu} \quad (2)$$

in which ν = kinematic viscosity of the fluid. The value of Re_d^* corresponds to the non-dimensional roughness height commonly adopted in recent literature as

$$k_s^+ = \frac{u^*k_s}{\nu} = 11.63 \frac{k_s}{\delta} \quad (3)$$

Both formulations are equivalent, in fact identical for $k_s = d$, and express the ratio of the roughness height k_s to the thickness δ of the viscous sublayer of the boundary layer.

The measured data on the initiation of motion form a band curve which marks the region between sporadic movement and full movement. Numerical results may only be determined from the Shields diagram iteratively. Owing to this, diverse empirical formulae have been developed to describe the behaviour represented by the Shields curve. Summaries of the extensive literature on the initiation of sediment motion may be found e.g. in Graf (1984), Yalin (1972), Simons/Sentuerk (1977), Zanke (1996). In recent decades the Shields curve has been discussed at great length and supplemented by new measurements. In the region $k_s^+ < 1$, backed up by only a small number of measurements by Shields, measurements by Mantz (1977) and Yalin/Karahan (1979) indicate that motion is initiated by considerably smaller shear stresses than interpreted by Shields on the basis of his measurements (see Fig. 1). Additional measurements have been conducted e.g. by Paxis (1976) and Unsoeld (1984). The measurements by Unsoeld are based on pure quartz sediments, which become cohesive in the extremely fine range without additional cohesive soil fractions. According to Unsoeld, this is the case for $d < 0.016$ mm.

2 ANALYTICAL SOLUTION

2.1 Initiation of Motion in Non-Turbulent Flow

The ratio F_T/F_W in Eq. 1 represents the angle of internal friction ϕ at the inception of motion

$$\frac{F_T}{F_W} = \tan \phi \quad (4)$$

For the critical state of the initiation of motion (subscript 'c') for natural sediments with a 70% solid fraction, Eq. 1 may also be expressed by

$$\tau_{c,eff}^* = 0.7 \tan \phi \quad (5)$$

The subscript 'eff' indicates that the actual local and instantaneous shear stress initiating motion on the bed is implied. For the case that a viscous, non-turbulent flow is effective above the bed, the initiation of motion is defined solely by Eq. 5.

The value of ϕ lies in the region of 30° for sand and attains about 45° for angular stones. On a sediment surface the layer of single grains is scattered and a certain proportion also exhibits smaller ϕ values. For this reason the bed may be set in motion gradually. In order to distinguish between the general angle of friction ϕ and local values, the latter is denoted in the following by ϕ' . The basic relationships considered in the following equally apply to ϕ' .

2.2 Initiation of Motion in Turbulent Flow

Under real conditions the shear stresses required to initiate motion only occur when the flow is

turbulent and when the viscous sublayer of the flow becomes so thin that the grains themselves more or less enter the region of turbulent action. This is accompanied by two additional effects:

1. The effective shear stress τ_{eff}^* actually responsible for the initiation of sediment motion is no longer directly but indirectly expressed by the time-averaged value $\bar{\tau}^*$ of the shear stress due to the fact that *additional shear stress fluctuations* $\tau'(t)$ occur (Fig. 2). In other words, the actual shear stress $\tau_{c,eff}^*$ initiating motion, depending on the degree of fluctuations, is always larger than the time-averaged shear stress. In the following, $\bar{\tau}^*$ is more simply denoted by τ^* .

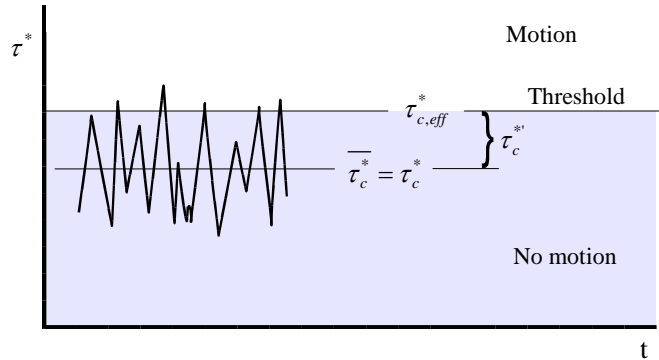


Fig. 2 The effective shear stress $\tau_{c,eff}^*$ and the shear stress τ_c^* averaged over time t responsible for the initiation of motion

2. Pressure fluctuations induced by turbulence give rise to lift forces acting on the grains. These turbulence-induced lift forces are mainly attributable to the coherent structures of the flow in the proximity of the wall. These are far more predominant than the lift forces generated by the curvature of streamlines of the flow over the grains. For this reason, the latter are not dealt with separately but are included in the overall lift forces.

2.2.1 Influence of turbulence-induced fluctuations τ' of the shear stress

From Fig. 2 the critical state is given by

$$\tau_c^* = \tau_{c,eff}^* - \tau_c^{*'} \quad (6)$$

and from Eq. 5

$$\tau_c^* = 0.7 \tan \phi - \tau_c^{*'} \quad (7)$$

Rearranging Eq. 6 and introducing $\tau = \rho \cdot u^2$ and $u^{*'}/u^* = (u'/u)_b$ leads to

$$\frac{\tau_c^{*'}}{\tau_c^*} = \frac{\tau_{c,eff}^* - \tau_c^*}{\tau_c^*} = \frac{(u + u'_c)^2 - u_b^2}{u_b^2} = \left(1 + \frac{u'_c}{u}\right)_b^2 - 1 \quad (8)$$

In the foregoing, $u^{*'}$ are the instantaneous fluctuations of the shear velocity at the bed, u_b and u'_b are the velocity and the fluctuation velocity at the bed, respectively, and u'_c is the instantaneous magnitude of u' responsible for the initiation of motion. Substituting Eq. 8 into Eq. 7 yields, as an intermediate result, the critical time-averaged shear stress for turbulent flow (still without the effects of lift forces):

$$\tau_c^* = \frac{\tau_{c,eff}^*}{\left(1 + \frac{u'_c}{u}\right)_b^2} = \frac{0.7 \tan \phi}{\left(1 + \frac{u'_c}{u}\right)_b^2} \quad (9)$$

2.2.2 Influence of the lift forces F_L

If the weight F_W of a sediment particle is reduced due to lift forces F_L , $F_{W,eff} = F_W - F_L$ and correspondingly lower shear forces F_T and lower shear stresses τ^* are required to initiate motion. These are given by the condition:

$$\frac{F_{T,required}}{F_T} = \frac{F_{W,eff}}{F_W} = \frac{F_W - F_L}{F_W} = 1 - \frac{F_L}{F_W} = \frac{\tau_{without_lift}^*}{\tau_{with_lift}^*} \quad (10)$$

The shear stresses required for initiating motion thus reduce to the same degree as the reduction in the effective particle weight. Taking this into consideration in Eq. 5 leads to

$$\tau_{c,eff}^* = 0.7 \tan \phi \cdot \left(1 - \frac{F_L}{F_W} \right) \quad (11)$$

or, extended by F_T to

$$\tau_{c,eff}^* = 0.7 \tan \phi \cdot \left(1 - \frac{F_L}{F_T} \cdot \frac{F_T}{F_W} \right) \quad (12)$$

which, on account of $F_T/F_W = \tan \phi = \tau^*/0.7$ (Eqs. 4 and 5), may also be written as

$$\tau_{c,eff}^* + \tau_{c,eff}^* \cdot \frac{F_L}{F_T} \cdot \tan \phi = 0.7 \tan \phi \quad (13)$$

Introducing the lift stress acting on the grain $\sigma_L = F_L/A$ over the effective surface A and with $\tau = F_T/A$, the following may also be written

$$\tau_{c,eff}^* = \frac{0.7 \tan \phi}{\left(1 + \frac{\sigma_L}{\tau} \tan \phi \right)} \quad (14)$$

This represents the shear stress initiating motion of the grain when lift forces become effective.

2.2.3 Fundamental equation for the initiation of motion in turbulent flow

From the basic Eq. 5, under consideration of the turbulence-induced shear stress peaks expressed by Eq. 9 and the lift forces expressed by Eq. 14, the *time-averaged critical shear stress* is given by:

$$\tau_c^* = \frac{0.7 \tan \phi}{\left(1 + \frac{u'_{c,b}}{u_b} \right)^2 \left(1 + \frac{\sigma_L}{\tau} \tan \phi \right)} \quad (15)$$

2.3 Alternative Solution for Single Grains

In the foregoing, the critical state was described by the angle of internal friction, which is here identical to the angle of repose. Instead of the general angle of repose ϕ the local angle of grain contact ϕ' may also be applied. This is illustrated in Fig. 3 by an exemplary sediment grain. The grain is labelled for the purpose of balancing forces and moments in relation to the angle ϕ' . The forces acting on the grain are the drag force F_D , the weight of the grain F_W and a lift force F_L .

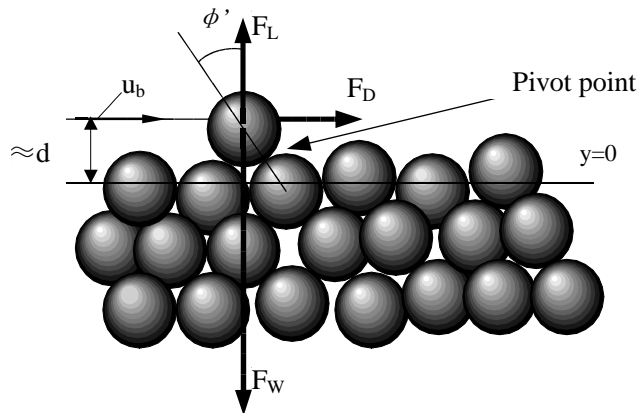


Fig. 3 Forces and notations for a single grain

The following forces act on the grain under consideration

$$F_D = c_D \rho \frac{1}{2} u_{b,eff}^2 A_{front} = c_D \rho \frac{1}{2} u_{b,eff}^2 k_D d^2 \cdot E \quad (16)$$

$$F_L = c_L \rho \frac{1}{2} u_{b,eff}^2 A_{ground} = c_L \rho \frac{1}{2} u_{b,eff}^2 k_L d^2 \quad (17)$$

$$F_W = (\rho_s - \rho) g V = (\rho_s - \rho) g k_W d^3 \quad (18)$$

Whereby c_D = the drag coefficient, c_L = the lift coefficient, $u_{b,eff} = u_b + u'_b$ = effective flow velocity acting on the grain, u_b = time-averaged flow velocity acting on the grain, u'_b = fluctuation of u at the grain, d = grain diameter, k_D = form factor (for spheres = $\pi/4$), k_L = form factor (for spheres = $\pi/4$), k_W = form factor (for spheres = $\pi/6$), E = degree of exposition (grain fully-embedded $E=0$, grain fully-exposed $E=1$, V =volume).

By balancing moments about the axis through the grain pivot points (owing to the three-dimensional layering, each grain has two pivot points) and by balancing forces (see e.g. also Graf, Simons/Sentuerk i.a.), the following is obtained

$$\frac{u_{b,c,eff}^2}{\rho' g d} = \frac{2 k_W \tan \phi'}{E \cdot k_D c_D + k_L c_L \tan \phi'} \quad (19)$$

If, analogous to Section 2.2, the effects of turbulence are also taken into account, this expression becomes

$$\frac{u_{b,c}^2}{\rho' g d} = \frac{2 k_W \tan \phi'}{\left(1 + \frac{u'}{u_b}\right)^2 (E \cdot k_D c_D + k_L c_L \tan \phi')} \quad (20)$$

Eq. 20 in combination with Eqs. 16 and 17 may be further rearranged to yield

$$\frac{u_{b,c}^2}{\rho' g d} = \frac{2 \tan \phi'}{c_D \frac{E \cdot k_D}{k_W} \left(1 + \frac{k_L c_L}{k_D c_D E} \tan \phi'\right) \cdot \left(1 + \frac{u'_{c,b}}{u_b}\right)^2} \quad (21)$$

With $(k_L \cdot c_L) / (k_D \cdot c_D \cdot E) = F_L / F_D$ this results in

$$\frac{u_{b,c}^2}{\rho' g d} = \frac{2 \tan \phi'}{c_D \frac{E \cdot k_D}{k_W} \left(1 + \frac{F_L}{F_D} \tan \phi'\right) \cdot \left(1 + \frac{u'_{c,b}}{u_b}\right)^2} \quad (22)$$

Introducing, on the one hand F_D according to Eq. 16, and on the other hand $F_D = \tau \cdot A = \tau \cdot d^2$ as well as $\tau = u^{*2} \rho$, initially yields $c_D \cdot u_b^2 = 2 u^{*2} / (E \cdot k_D)$, which then leads to

$$\frac{u_c^{*2}}{\rho' g d} = \tau_c^* = \frac{k_W \tan \phi'}{\left(1 + \frac{u'_{c,b}}{u_b}\right)^2 \cdot \left(1 + \frac{F_L}{F_D} \tan \phi'\right)} \quad (23)$$

Balancing moments for a single grain thus leads to a formally identical result to that obtained from a formulation based on the internal angle of friction (Eq. 15). (Note: F_D in Eq. 23 is given by Eq. 16, which means that the exposition E of a single grain is included at this point). The factor 0.7 appearing in Eq. 15 is given here by k_W , which corresponds to $k_W = 0.52$ for spheres. Under natural conditions the grain layering is three-dimensional and sediment particles are not perfectly spherical. An exposition of less than 1 leads to a somewhat larger value of τ_c^* . This means that the constant factor is here subject to slight deviations. **Of prime importance is the fact that the internal angle of friction ϕ and the angle of grain contact ϕ' are equivalent and may be equally applied with regard to the initiation of motion.**

2.4 Formulation for u' / u_b

In order to solve Eqs. 15 and 23 an expression for $(u'/u)_b = f(k_S^+)$ is required, as the measurements presented in Fig. 1 are a function of $Re_d^* = k_S^+$. This relationship is not documented in the literature. The

literature does, however, provide information on a) u'/u^* and b) u_b/u^* via the universal velocity distribution law. For this reason, $(u'/u)_b$ is determined in the following by an alternative method based on the quotients

$$\frac{u'_b/u^*}{u_b/u^*} = \frac{u'_b}{u_b} \quad (24)$$

The literature provides additional information referred to the temporally constant velocity fluctuations u'_{rms} ($\sqrt{\overline{u'^2}}$ = standard deviation of $u'(t)$) in the form

$$\overline{u'^2} = \frac{1}{T} \int_{t=0}^T (u'(t))^2 dt \quad (25)$$

The effective values of u'_c responsible for initiating motion are a multiple of u'_{rms} to be determined at a later stage:

$$u'_c = n \cdot u'_{rms} \quad (26)$$

The value of n defines $u' = u'_c$ for the initiation of motion compared with u'_{rms} . On account of the behaviour of the Gaussian curve for the probability of occurrence of values larger than u' , it is possible to restrict n within the range $0 < n < 3$ (Fig. 4).

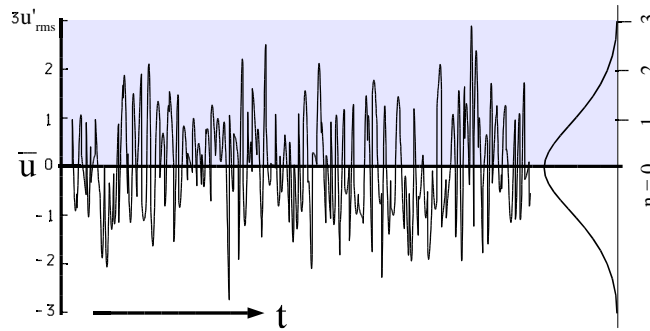


Fig. 4 Regarding the definition of n

Diverse results of measurements may be found in the literature concerning the relationship $u'_{rms}/u^* = f(y^+)$, whereby $y^+ = u^* y/\nu$ and y = distance from the wall. No information is available, however, on the relationship required here as a function of k_s^+ . According to Nezu and Rodi (1986) the results of measurements by different authors (Laufer, Grass, Eckelmann, Nakagawa/Nezu, Steffler, Rajaratnam, Peterson as well as Nezu and Rodi) may be described by the following semi-empirical equation for smooth walls

$$\frac{u'_{rms}(y^+)}{u^*} = 0.3 \cdot y^+ \cdot e^{-0.1y^+} + 2.26 \cdot e^{-\frac{0.88y^+}{h}} \cdot (1 - e^{-0.1y^+}) \quad (27)$$

(Note: provided $h/d > \text{approx. } 100$, $e^{-0.88 d/h} \approx 1$).

The term $(1 - e^{-0.1y^+})$ in Eq. 27 is the modified van Driest damping coefficient after Nezu/Rodi. Nezu and Nakagawa (1993) present the results of measurements by Grass (1971) and Nezu (1977) for $u'_{rms,y}/u^* = f(y^+)$ for different roughness states k_s^+ . From this bunch of curves the behaviour of the sought function $u'_{rms}/u^* = f(k_s^+)$ may be derived for $y = k_s$, or equivalently $y^+ = k_s^+$, and the curve may be described to a high degree of accuracy by modifying the factors in Eq. 27 (Fig. 5) as

$$\frac{u'_{rms}(y = k_s)}{u^*} = \frac{u'_{rms,b}}{u^*} = 0.31 \cdot k_s^+ \cdot e^{-0.1k_s^+} + 1.8 \cdot e^{-\frac{0.88d}{h}} \cdot (1 - e^{-0.1k_s^+}) \quad (28)$$

The universal velocity distribution law may be approximately expressed by Eq. 29 (Zanke, 1996)

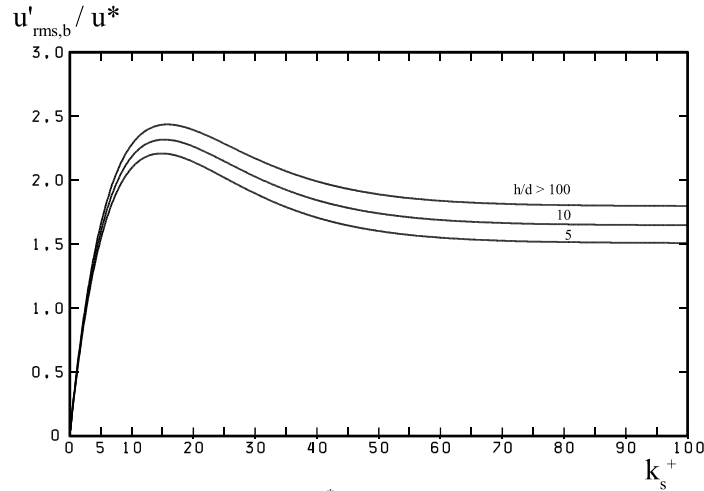


Fig. 5 $(u'_{rms}/u^*)_b = f(k_s^+)$ after Eq. 28

$$\frac{u_y}{u^*} = \left(\frac{1 - P_t}{k_s^{+2}} + \frac{P_t}{\left(2.5 \ln \frac{y}{k_s} + B \right)^2} \right)^{-0.5} \quad (29)$$

For the bed, denoted by the subscript b, the substitution $y=d=k_s$ is adopted here (see above and Fig. 3). Only the integration constant B is then retained in the denominator of the second addend.

In Eq. 29 the expression

$$P_t = 1 - e^{-0.08 k_s^+} \quad (30)$$

states the probability that the flow is turbulent and is thus related to the von Driest damping coefficient. After Zanke 1996, B may be approximated for the sand-roughness case by

$$B_{sandrough} = (1 - P_t) \cdot (2.5 \ln(k_s^+) + 5.25) + P_t \cdot 8.5 \quad (31)$$

(Note: by adopting naturally rough conditions instead of sand roughness and thus using

$$B_{nat.rough} = 2.5 \ln \left(\frac{1}{0.033 + \frac{0.11}{k_s^+}} \right) \quad (31a)$$

only slight differences arise in the results presented in the following)

By this means it is possible to determine $(u'_{rms}/u)_b$ using Eq. 24 in combination with Eqs. 28 and 29. In the fully-turbulent region a value of $u_b/u^* = 8.5$ is obtained for an effective distance from the bed of $y = d = k_s$. On the other hand, $u'_{rms,b}/u^* = 1.8$ (see Fig. 5, for $h/d > 100$). This means that $(u'_{rms}/u)_{b,rough} \approx 1.8/8.5 \approx 21\% = \text{const.}$ in the rough region. In the region of smaller k_s^+ , where the grains lie within the viscous sublayer of the boundary layer, the values of u_b/u^* computed in this manner increase to approx. 0.5 (Fig. 6). The latter is almost improbable and may be attributed to the fact that the slight inaccuracies in the semi-empirical solutions for u_b'/u^* and u_b/u^* are amplified, especially because u_b (in the denominator in Eq. 24) approaches 0 at the wall. Measurements of $(u'_{rms}/u)_b$ have been carried out on smooth walls by Eckelmann (Hinze, 1975), albeit as a function of the distances from the wall y^+ and not as a function of k_s^+ . According to these measurements the values of $(u'_{rms}/u)_b$ increase on approaching the wall and attain a maximum at about $y^+ = 4$, with a maximum value of approx. 0.38. Approaching the wall further, the values again decrease, whereby a finite value of about $(u'_{rms}/u)_b \approx 0.24$ as well as a value approaching zero are interpretable from measurements directly adjacent to the wall. In order to apply these results to the dependency of k_s^+ , analogous to the transition from Eq.27 to Eq. 28, measurements are lacking regarding

the behaviour for different wall roughnesses. For this reason, alternative criteria must be sought. Such a criterion is the necessity that the behaviour of $(u'_{rms}/u)_b = f(k_s^+)$ for $k_s^+ \rightarrow 0$ transforms into the behaviour of $(u'_{rms}/u)_b = f(y^+)$ at the smooth wall. As the function $(u'_{rms}/u)_b = f(y^+)$ for the smooth wall, as previously mentioned, attains a maximum in the proximity of the wall and that smaller values occur directly at the wall, this is also expected for the sought function $(u'_{rms}/u)_b = f(k_s^+)$. According to Dittrich (1998) a finite velocity still exists above rough beds at the origin of the universal velocity profile. If a shift of the origin in the proximity of the wall (empirical) is applied

$$\frac{u_b}{u^*} = 0.8 + 0.9 \frac{u_{y=k_s}}{u^*} \quad (32)$$

it is found that Eq. 24 gives plausible values for $(u'_{rms}/u)_b$, which reflects the essence of the results obtained by Eckelmann (see Fig. 6). The difference between the two possible solutions for $(u'_{rms}/u)_b$ shown in Fig. 6 is only apparent in the region of $k_s^+ < \text{approx. } 5$. Comparative calculations show that acceptable results for τ_c^* are obtained even for a constant value of $(u'_{rms}/u)_b$.

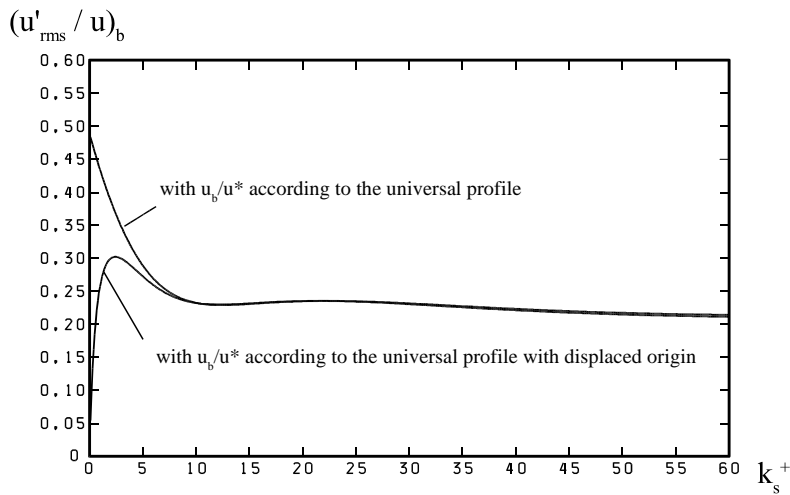


Fig. 6 Behaviour of $(u'_{rms}/u)_b$ as a function of k

2.5 Formulation for $F_L / F_T = \sigma_L / \tau$

Lift forces develop at sediment grains due to pressure differences between the upper and lower surfaces of the grain. These may be caused by two effects:

1. dynamic lift due to the curvature of streamlines and
2. turbulence-induced pressure differences.

Dynamic lift (effects of streamline curvature) only occurs at grains which are fully-exposed and cause a significant increase in the flow path over the upper surface of the grain. In the case of other grains the dynamic lift is of minor importance or non-existent. Due to turbulence, velocity peaks occur on the grain upper surfaces, which correlate with pressure reduction events (whereby $p_{rms} u'^2_{rms}$). On the lower surface of the grain this effect is only slight or non-existent due to embedding, leading to pressure differences Δp in the vertical direction of the grain. The lift stress is $\sigma_L = \Delta p$. The instationary turbulence-induced lift stresses $\sigma_{L,rms}$ acting on a grain ($\sigma_L = F_L/A = \text{lift force per unit area}$) may thus be expressed by

$$\sigma_{L,rms} = const \cdot \rho u'^2_{rms,b} \quad (33)$$

(see corresponding formulation for maximum values of σ_L in Dittrich 1998, page 166). Owing to the fact that $\tau = u^{*2} \cdot \rho$, the following holds

$$\sigma_{L,rms} / \tau = c \left(u'^2_{rms} / u^{*2} \right)_b \quad (34)$$

According to different authors (see Hinze 1975 and Dittrich 1996) the value of $(\sigma_L / \tau)_{max}$ lies between

approx. 2 and 3. According to Fig. 5, on the other hand, $(u'_{rms}/u^*)_{\max} \approx 2.5$, which initially leads to

$$\frac{F_L}{F_D} = \frac{\sigma_L}{\tau} = \frac{1}{2.5} \cdot \left(n \cdot \frac{u'_{rms,b}}{u^*} \right)^2 \quad (35)$$

for $c \approx 1/2.5$. Taking into consideration Eqns. 26 and 35, Eq. 15 may thus be expressed as

$$\tau_c^* = \frac{0.7 \cdot \tan \phi}{\left(1 + n \cdot \frac{u'_{rms,b}}{u_b} \right)^2 \cdot \left(1 + \frac{1}{2.5} \left(n \cdot \frac{u'_{rms,b}}{u^*} \right)^2 \tan \phi \right)} \quad (15a)$$

(u'_{rms}/u^* from Eq. 28 and u_b/u^* from Eq. 32). In accordance with Section 2.3 the individual angle of grain contact ϕ' may be applied in place of ϕ .

2.6 Influence of Cohesive Action

In the range of very fine grains, cohesive action occurs in the quartz-water system. This may be accounted for e.g. as an apparent additional density ρ_{SS} . The density included in the formulation is then $\rho_{S,eff} = \rho_S + \rho_{SS}$. A semi-empirical expression for ρ_{SS} is

$$\rho_{SS} = \frac{const}{d^2} \quad (36)$$

With d expressed in (m), ρ_{SS} is given in (kg/m^3). Based on measurements by Unsoeld (Fig. 7) for the quartz-water system, the value of 'const.' is found to be $\approx 3 \cdot 10^{-8} \text{ kg}/\text{m}$. Alternatively, the cohesive effect may also be taken into account by increasing the angle of internal friction. This leads to

$$K = \frac{\tan \phi_{eff}}{\tan \phi} = \frac{F_{W,eff}}{F_W} = \frac{\rho_S - \rho + \rho_{SS}}{\rho_S - \rho} = \left(1 + \frac{\rho_{SS}}{\rho_S - \rho} \right) = \left(1 + \frac{3 \times 10^{-8} [\text{kg} / \text{m}]}{(\rho_S - \rho) \cdot d^2} \right) \quad (37)$$

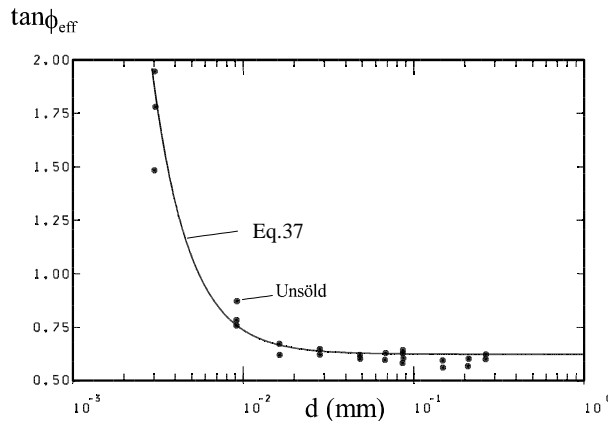


Fig. 7 $\tan \phi_{eff}$ as a function of the cohesive action of the quartz-water system based on measurements by Unsoeld (1984) and Eq. 37

If cohesion is present, $\tan \phi$ must be replaced by $\tan \phi_{eff}$ in Eqns. 15, 15a,b,c. Cohesive action due to cohesive fractions in the sediment leads to an additional increase in $\tan \phi$, expressed by a displacement of the curve given in Fig. 7 to the right. Fig. 7 shows measured values by Unsoeld together with the curve derived from Eq. 37 (angle of repose in the cohesion-free region in Fig. 7 is approx. $\phi = 32^\circ$).

3 RESULTS

3.1 Solution for the Shields Curve

The grains on the bed occupy a multitude of different positions and are subject to turbulence-induced fluctuating shear and lift stresses. With the corresponding probability distributions, and on the basis of Eq.

15a, the overall initiation of motion may be simulated between 0% and 100% probability of motion by applying statistical methods. These distributions are not known in the first instance. For each degree of movement, however, value combinations of the turbulent fluctuation velocities and the local angle of friction $\phi' < \phi$ may be found. Out of this spectrum the Shields curve describes a specific weak degree of motion which according to Zanke (1990) is approximately 10%.

Taking the combination of e.g. $n \approx 1.8$ and $\phi' \approx 20^\circ$ as representative values, Eq. 15a maps the Shields curve (Fig. 8). This may thus be expressed by

$$\tau_{c, Shields}^* = \frac{0.24 \cdot K}{\left(1 + 1.8 \cdot \frac{u'_{rms,b}}{u_b}\right)^2 \cdot \left(1 + 0.14 \left(1.8 \cdot \frac{u'_{rms,b}}{u^*}\right)^2 K\right)} \quad (15b)$$

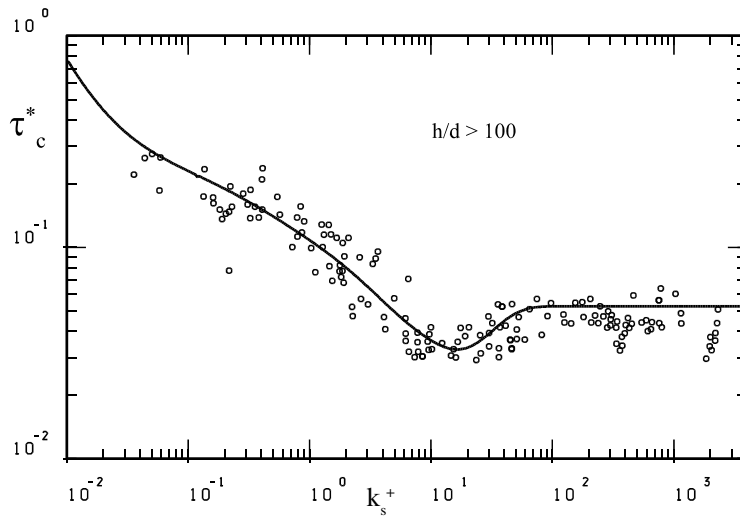


Fig. 8 Measured data on the initiation of motion including the curve derived from Eq.15b

By considering the general limiting angle of repose ϕ of the sediment, which is about 30° for sand, and may attain as much as 45° for angular stones, the following may also be formulated

$$\tau_c^* = \frac{0.7 \cdot \tan(\phi/1.5) \cdot K}{\left(1 + 1.8 \cdot \frac{u'_{rms,b}}{u_b}\right)^2 \cdot \left(1 + 0.4 \left(1.8 \cdot \frac{u'_{rms,b}}{u^*}\right)^2 \cdot \tan(\phi/1.5) \cdot K\right)} \quad (15c)$$

For grain sizes of approx. $d > 0.02\text{mm}$, $K=1$. In the case of finer sediment, cohesive effects according to Eq. 37 also play a role. In (15c) $\phi/1.5 = \phi'$, i.e. for a general $\phi=30^\circ$ a representative value of $\phi'=20^\circ$ takes into account that the grains at Shields critical condition have local $\phi' < \phi$.

3.2 Analysis of the Effects of Turbulence on the Initiation of Motion

The effects of shear stress fluctuations (Fig. 2) as well as fluctuations in the lift forces are shown in Fig. 9. Both effects reduce the shear stresses required to initiate motion from a constant value of 0.24 in the absence of turbulence to the form of the Shields curve. The effect of shear stress peaks is illustrated in the figure by (a), whereas (b) shows the reduction in the shear stresses required to initiate motion as a result of lift forces. (The reference curve “without turbulence” is not possible in reality as only turbulent flows can provide the forces necessary to initiate motion).

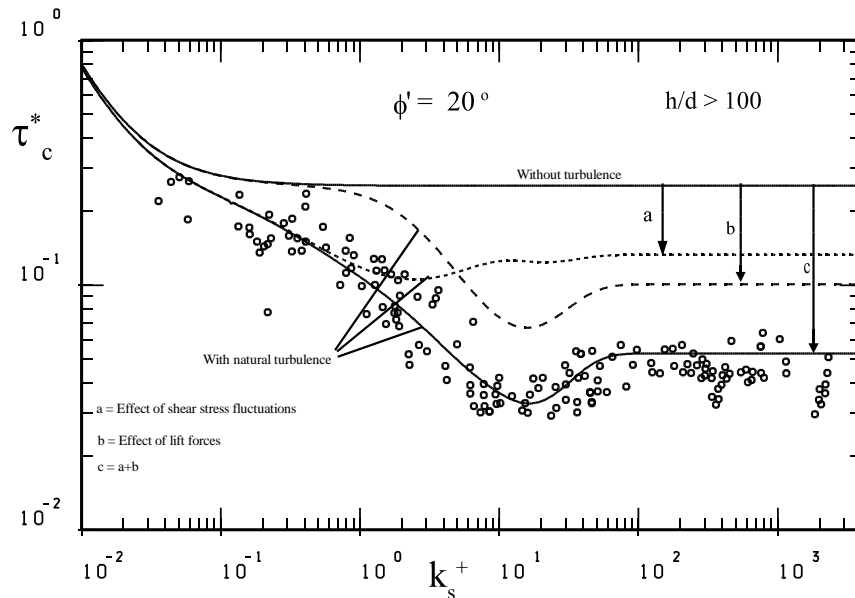


Fig. 9 Critical shear stresses for non-turbulent flow ($u'=0$) and a flow with “normal” turbulence

3.3 Effects of Grain Contact Angle, Degree of Turbulence, Cohesion and Relative Water Depth h/d on the Initiation of Motion

In the following figures the influence of the individual effects of the angle of internal friction (or the angle of contact between grains), the degree of turbulence, cohesive forces and the relative water depth h/d are presented on the basis of Eq. 15a. Fig. 10 shows the influence of ϕ . Larger angles of friction or grain contact angles lead to higher critical shear stresses, whereby the effect for small k_s^+ is greater than

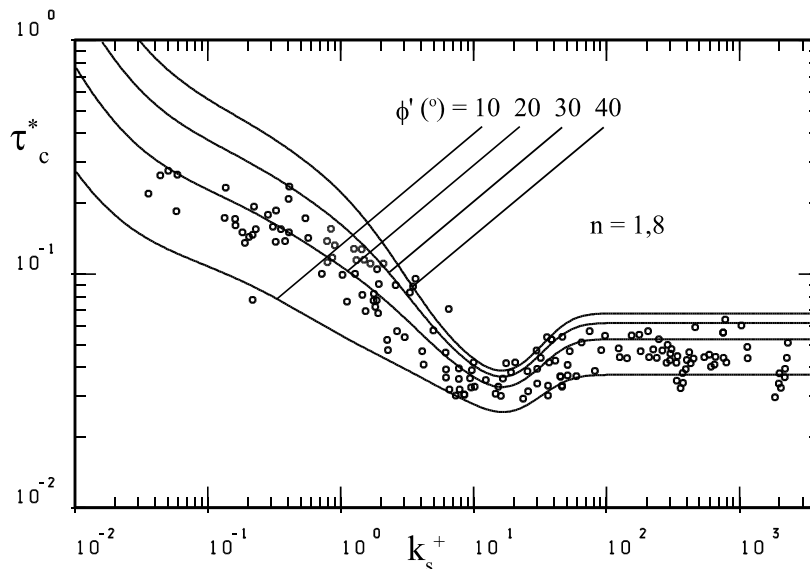


Fig. 10 Effect of different angles of repose ϕ (or correspondingly different angles of grain contact ϕ')

in the hydraulically rough region in which $k_s^+ > \text{approx. } 70$. Fig. 11 indicates the way in which the initiation of motion is promoted by turbulence-enhancing effects (e.g. structures) at low flow rates. Due to the viscous sublayer of the boundary layer these effects are damped on moving towards the fine-grain

region. The dashed line indicates the initiation of motion in the absence of the viscous sublayer. Fig. 12 illustrates the action of cohesion in the quartz-water system, which becomes effective at approx. $k_s^+ < 0,5$ and increases the resistance of sediment to movement. The influence of low relative water depths h/d in Fig. 13 is explained by Eq. 28. With decreasing relative water depth the required shear stress increases (i.e. the load on the bed reduces for otherwise constant conditions), whereby this effect decreases significantly on moving towards the hydraulically smooth region and practically disappears at $k_s^+ = 0,1$. This effect also disappears for values of $h/d > \text{approx. } 100$. With regard to the latter, the results obtained from Eq. 15a are verified by the measurements of Bayazit (1982, Fig. 14).

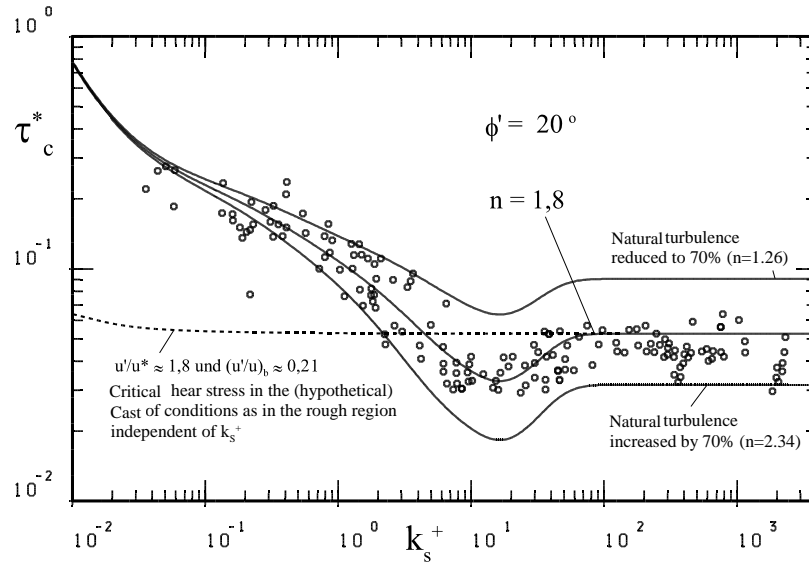


Fig. 11 Effect of damped and enhanced turbulence

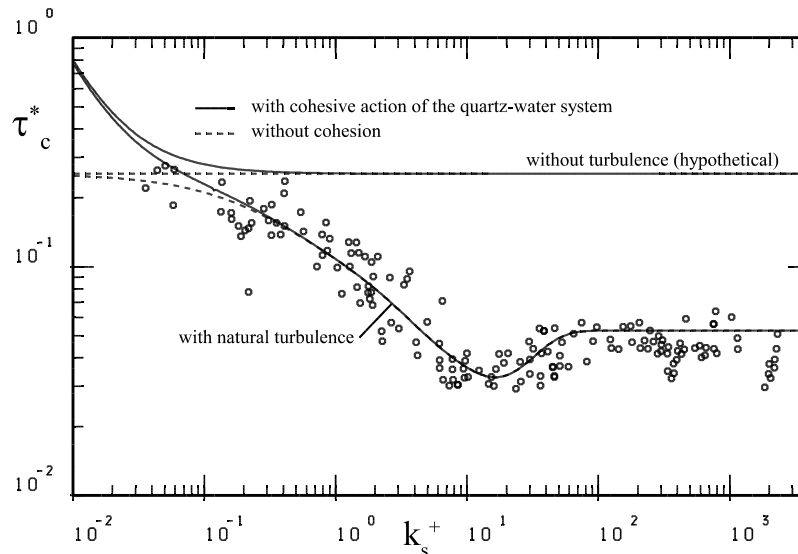


Fig. 12 Effect of cohesive action

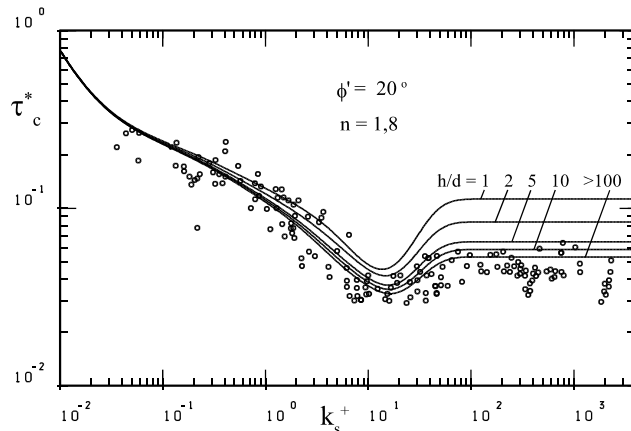


Fig. 13 Effect of relative water depth h/d

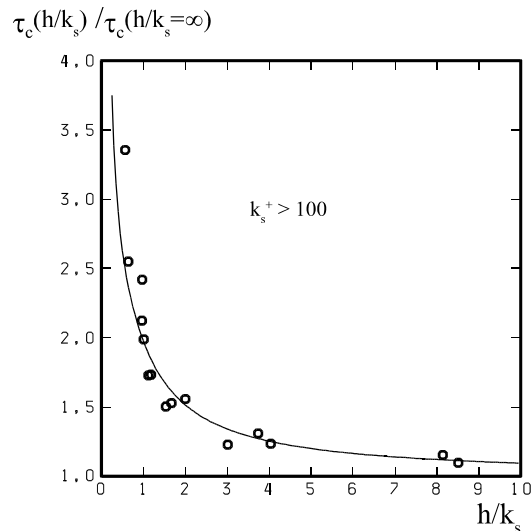


Fig. 14 Relationship between the critical shear stress and the relative water depth (= relative water cover) after measurements by Bayazit 1982 (in Ditttrich, 1998) as well as the curve computed from Eq. 15a for $k_s^+ > 100$

4 SUMMARY

The decisive factor for the initiation of sediment motion is the mechanical mobility of sediments. This is given e.g. by the angle of internal friction, which is identical to the limiting angle of repose ϕ for cohesionless sediments, and may be applied either locally or to the entire bed. Alternatively and equally applicable, the angle of grain contact ϕ' for an individual grain may also be introduced. In non-turbulent flow $\tau_c^* = \text{const} \cdot \tan\phi$ (or $\tau_c^* = \text{const}_1 \tan\phi'$) would thus apply. In the range of very fine sediments the angle ϕ or ϕ' is increased due to cohesion effects.

In turbulent flow, two additional effects must be considered:

1. The effective shear stress acting on a grain is increased above the time-averaged shear stress owing to turbulent stress peaks and
2. The grains exposed to the flow become effectively lighter due to lift forces.

Both of these turbulence-induced effects are randomly distributed. With a knowledge of the pertinent distributions it would be possible to simulate the initiation of motion statistically by the random combination of an individual grain contact angle with a local instantaneous turbulence regime. These distribution functions, especially those relating to the probability of a particular grain attitude, under

consideration of the three-dimensional nature of grain layering, are still the subject of present research. In this paper the initiation of motion is thus defined in the first instance by representative (governing) values of the grain contact angle and the fluctuation velocity u' responsible for initiating motion (given by the factor n), which may be traced back to the degree of motion represented in the Shields curve.

Finally, the effects of different angles of internal friction (corresponding to different angles of grain contact), degrees of turbulence in the flow, cohesive action in the sediment and relative water cover heights h/d are analysed and presented on the basis of Eq. 15a. Of special mention is the significant influence of turbulence (Fig. 11). A good fit was also obtained between the computed results for different relative water covers and the measurements of Bayazit (Fig. 14).

In order to avoid misunderstandings, the significance of the value of ϕ' entered in the foregoing figures is explained here in more detail. ϕ' relates to a particular portion of the sediment surface, set in motion by a particular degree of turbulence, given here by the value n , under the action of an averaged non-dimensional shear stress τ_c^* . For natural sediments, which form the basis of the measurements plotted in the figures, the general angle of repose (= the general angle of internal friction) is about 30° . The more easily mobilized fractions with a 20° grain contact angle constitute a relevant percentage with regard to the initiation of motion. In the case of revetments with stone chippings, for example, with a general angle of internal friction of approx. up to 45° , this fraction is smaller, and the initiation of motion first occurs under higher flow loading.

In this paper the underlying mechanisms responsible for the initiation of sediment motion have been analysed. Greater precision in forecasting the initiation of motion may be expected from an investigation of the probability distribution of ϕ' and the influence of three-dimensional layering.

REFERENCES

- Casey, H. J. 1935, Ueber Geschiebebewegung (On Bed Load, in German). Mitt. Preuss. Versuchsanstalt f. Wasserbau u. Schiffbau, Berlin
- Bayazit, M. 1982, Flow structure and sediment transport mechanics in steep channels. Mechanics of Sediment Transport, Proc. of EUROMECH 156, Istanbul
- Dittrich, A. 1996, Ratio of Lift and Shear Forces over Rough Surfaces. in: Coherent Flow Structures, John Wiley
- Dittrich, A. 1998, Wechselwirkung Morphologie/Stroemung naturnaher Fliessgewaesser (Interaction between Morphology and Current in natural rivers, in German). Mitt. Inst. für Wasserwirtschaft u. Kulturtechnik, Univ. Karlsruhe, Heft 198
- Graf, W. H. 1984, Hydraulics of Sediment Transport. Water Resources Publication, Littleton, Colorado
- Hinze, J. O. 1975, Turbulence, McGraw-Hill Book Comp.
- Kramer, H. 1932, Modellgeschiebe und Schleppkraft (Model Sediment and Shear Force, in German). Berlin
- Nezu, I. U. and Rodi, W. 1986, Open Channel Flow Measurements with a Laser Doppler Anemometer. ASCE, Journal Hyd. Eng., Vol. 112, No. 5
- Nezu, I. U. and Nakagawa, H. 1993, Turbulence in Open Channel Flows. IAHR Monograph, A.A. Balkema
- Mantz, P.A. 1977, Incipient Motion of Fine Grains and Flakes by Fluids - Extended Shields-Diagram. ASCE, Journal Hyd. Div., Vol 103, HY 6
- Pazis, G. C. 1976, Faible transport des sediments par erosion et deposition dans des canaux alluvionaires. These de doctorat, Ecole Polytechnique Federale de Lausanne, Suisse
- Shields, A. 1936, Anwendung der Aehnlichkeitsmechanik und der Turbulenzforschung auf die Geschiebebewegung. Mitt. Preuss. Versuchsanstalt fuer Wasserbau, Heft 26
- Simons, D.B. U. and Sentuerk, F. 1977, Sediment Transport Technolog., Water Recources Publications, Fort Collins, Colorado
- Yalin, M.S. 1972, Mechanics of Sediment Transport. Pergamon Press, Braunschweig
- Yalin, M.S. U. and Karahan, E. 1979, Inception of Sediment Transport. ASCE, Journal Hyd. Div., Vol 105, HY 11
- Unsoeld, G. 1984, Der Transportbeginn rolligen Sohlmaterials in gleichfoermigen turbulenten Stroemungen- Eine kritische Ueberpruefung der Shields -Funktion und ihre experimentelle Erweiterung auf feinkoernige, nichtbindige Sedimente (The Beginning of Motion of Cohesionless Sediment in Uniform Turbulant Flows- A Critical Check of Shields Function and an experimental Extension for Fine Grained Sediments in Uniform Turbulent Flows, in German). Diss. Univ. Kiel, Germany
- Zanke, U. 1990, Der Beginn der Sedimentbewegung als Wahrscheinlichkeitsproblem (The Beginning of Sediment Motion as a Probability Problem, in German). Wasser & Boden, Heft 1
- Zanke, U. 1996, Loesungen fuer das universelle Geschwindigkeitsverteilungsgesetz und die Shields-Kurve (Solutions for the Universal Velocity Distribution Law and for the Shields Curve, in German). Wasser und Boden, Heft 9

LIST OF SYMBOLS

| | |
|------------------|--|
| A | = area |
| c_D | = drag coefficient |
| c_L | = lift coefficient |
| d | = grain diameter |
| E | = degree of exposition (grain fully-embedded E=0, fully-exposed E=1) |
| F_D | = drag force on a body, here on a grain on the bed surface |
| F_T | = τA = effective shear force on the bed over the area A |
| F_L | = lift force |
| F_W | = weight of the initially mobilized surface referred to A |
| $F_{W,eff}$ | = $F_W - F_L$ |
| g | = gravitational acceleration |
| h | = water depth |
| k_D | = form factor (for spheres = $\pi/4$) |
| k_L | = form factor (for spheres = $\pi/4$) |
| k_W | = form factor (for spheres = $\pi/6$) |
| k | = roughness height (for natural sediments = d) |
| k_S | = equivalent sand roughness height = const d (here const = 1) |
| k_S^+ | = non-dimensional roughness height = $u^* k_S / \nu = 11.63 k_S / \delta$ |
| n | = factor, multiple of u'_{rms} |
| R | = risk of motion (=probability that grains move) |
| Re_d^* | = grain Reynold's number = $u^* d / \nu = 11.63 d / \delta$; for $k_S = d \rightarrow k_S^+ = Re_d^*$ |
| t | = time |
| u | = time-averaged value of the flow velocity at a wall distance indicated by subscript |
| u_b | = time-averaged velocity at a grain |
| $u_{b,eff}$ | = $u_b + u'_b$ effective flow velocity at a grain |
| $u'(t)$ | = instantaneous deviation from u, where $u'(t) = u(t) - u$ |
| u'_c | = for existing time-averaged $u = u_c$, the fluctuation value = $n u'_{rms}$ |
| u'_{rms} | = $\sqrt{u'^2}$ = standard deviation of $u'(t)$ |
| u'_b | = u' at the grain height |
| $u'_{max}(t)$ | = peak values of velocity fluctuations |
| u^* | = shear velocity |
| y | = distance from wall |
| y^+ | = non-dimensional distance from wall = $u^* y / \nu = 11.63 y / \delta$ |
| δ | = thickness of the viscous sublayer of the boundary layer, defined by $11.63 \nu / u^*$ |
| ϕ | = angle of internal friction (for complete water saturation or complete dryness = angle of repose), locally or globally applicable |
| ϕ' | = angle of grain contact or angle of friction for an individual grain |
| ρ | = fluid density |
| ρ_S | = sediment density |
| ρ' | = relative density = $(\rho_S - \rho) / \rho$ |
| ρ_{SS} | = apparent additional density of the sediment due to cohesive action |
| ν | = kinematic viscosity of the fluid |
| σ_L | = lift stress acting on a grain |
| τ | = shear stress at the bed (time-averaged value) |
| τ' | = shear stress fluctuation |
| τ^* | = non-dimensional shear stress = $\tau / ((\rho_S - \rho) g d = u^{*2} / (\rho^* g d)$, time-averaged value |
| $\tau^{*'}_i$ | = non-dimensional shear stress fluctuation |
| τ^*_{eff} | = $\tau^* + \tau^{*'}_i$ = effective non-dimensional shear stress |
| τ^*_c | = critical non-dimensional shear stress |
| $\tau^*_{c,eff}$ | = $\tau^*_c + \tau^{*'}_{c'}$ = effective non-dimensional critical shear stress |

Subscripts

| | |
|-----|--------------------------|
| b | = at the bed |
| rms | = root mean square value |